7th International Conference on Silicon Photovoltaics, SiliconPV 2017

Comparative study of differently grown tunnel oxides for p-type passivating contacts

Rik van der Vossen[a]*, Frank Feldmann[a], Anamaria Moldovan[a], Martin Hermle[a]

aFraunhofer ISE, Heidenhofstraße 2, 79110 Freiburg im Breisgau, Germany

Abstract

In this study, boron-doped passivating contacts are investigated. The focus of this study lies on comparing four different methods for growing the thin SiO_x tunnel layer, in order to better understand the relationship between the contact's surface passivation and contact resistivity. The thin oxide layers were grown in (i) boiling HNO_3 (ChemOx), (ii) by UV induced photo-oxidation (UV/O_3), (iii) by wet-chemical oxidation in ozonated water (O_3), and by a thermal oxidation (TO) process. All oxides show a similar thickness of around 1.2-1.4 nm. The thermal oxide proved to block the penetration of dopants more effectively than the other three oxides, which resulted in superior passivation. On planar silicon surfaces a saturation current density of 15 fA/cm^2 was achieved for the thermally grown oxide. Furthermore, the TO showed tolerance to higher annealing temperatures. The contact resistance of the analyzed samples was within a range where no significant fill factor losses are to be expected for full area cell contacts (< 100 $m\Omega cm^2$).

© 2017 The Authors. Published by Elsevier Ltd.
Peer review by the scientific conference committee of SiliconPV 2017 under responsibility of PSE AG.

Keywords: tunneling oxides; passivating contacts; TOPCon; contact resistivity

1. Introduction

Passivating and carrier-selective contacts have contributed significantly to increasing solar cell efficiency, which is important for levelized cost of electricity (LCOE) reduction. Multiple concepts have yielded promising results in order to achieve this. Yoshikawa et al. currently hold the world-record with 26.6% efficiency in the field of Si solar

---

* Corresponding author. Tel.: +49 (0) 7 61/ 45 88-5201.
 E-mail address: rik.van.der.vossen@ise.fraunhofer.de

cells by merging heterojunction technology with an IBC cell structure [1]. Another promising concept that shows good passivation qualities is poly-silicon contacts, which yield low saturation current densities and high open-circuit voltages [2,3]. The passivating contact investigated in this work features a thin tunnel oxide layer and a doped nano-crystalline silicon layer.

The TOPCon concept, developed by Feldmann et al. [4], has demonstrated a conversion efficiency of 25.7% on an *n*-type lab cell featuring a passivated rear contact [5]. This cell concept offers two benefits over cells with a partial rear contact (PRC): (i) extremely low recombination at the rear and (ii) a one-dimensional carrier flow in the base allowing higher fill factors. Remarkably low J_0 values of ~1 fA/cm² have been reported for *n*-type poly-Si/SiO$_x$ passivating contacts but *p*-type poly-Si contacts still show higher saturation current densities [2,3]. In an attempt to better understand the inferior behavior for boron doped contacts, the surface passivation and contact resistivity of the *p*-type passivating contact featuring four distinctively grown oxide layers are characterized.

2. Experimental details

2.1. Lifetime sample preparation

For the lifetime samples, 10 Ωcm *p*-type planar float zone (FZ) wafers with a thickness of 250 μm were cleaned according to the RCA procedure. After the RCA cleaning, each wafer received a dip in hydrofluoric acid (HF) to remove the oxide grown during the cleaning process. Thereafter, a tunnel oxide was grown on the wafers using (i) boiling HNO$_3$ (ChemOx), (ii) by UV induced photo-oxidation (UV/O$_3$), (iii) by wet-chemical oxidation in ozonated water (O$_3$), and a thermal oxidation (TO). Details for the ChemOx and UV/O$_3$ processes can be found in the work of Kobayashi et al. [6] and Moldovan et al. [7]. For the O$_3$ oxide, the wafers were submerged in a tank in which O$_3$ was dissolved in DI-water which contains an ozone concentration of 40 ppm at a temperature of 45 °C for 10 minutes. The oxidation reaction in ozonated DI-water is similar to the dry oxidation during the UV/O$_3$ process, which is described in the paper by Fink et al [8]. During the UV/O$_3$ oxide growth, the wafers are exposed to and UV excimer source, which emits monochromatic light at a wavelength of 172 nm. All of the mentioned methods resulted in an oxide with approximately 1.2 nm thickness, which was determined with spectral ellipsometry. Finally, thermal oxides having a thickness of about 1.4 nm were grown in a tube furnace at 600 °C for 10 minutes with a feed of N$_2$ and O$_2$ gas.

On top of the thin oxide layer, a stack consisting a thin intrinsic a-Si layer; followed by a boron doped a-Si layer and finally a SiC capping layer was deposited in the AK400M PECVD reactor from Roth & Rau. The thickness of these layers were approximately 4, 10 and 4 nm, respectively. The samples were annealed in a tube furnace at four different temperatures ranging from 850-1000 °C under N$_2$ atmosphere for 10 minutes. Finally, samples were passivated with remote plasma hydrogen passivation (RPHP) at 400 °C for 30 min [9]. For contact resistivity measurements linear and circular transfer length method (TLM) structures were realized on the samples by thermal evaporation of a stack of 50 nm titanium, 50 nm palladium and 300 nm silver, hereafter indicated with TiPdAg.

2.2. Measurement methodology

The samples were characterized by quasi steady-state photo conductance (QSSPC) measurements conducted on a WCT120 lifetime tester produced by Sinton Instruments [10]. The 10 Ωcm planar wafers were used to extract the saturation current density using the high injection method [11,12]. The samples were measured after the high-temperature anneal and once more after the hydrogen passivation to monitor the effect of the RPHP step. The dopant profiles were determined using electrochemical capacitance-voltage (ECV) measurements. The dopant profiles obtained during these measurements were then analysed using the freeware tool EDNA developed by McIntosh et al. [13] to simulate the effective surface recombination velocity based on the saturation current densities determined with the QSSPC measurements.

The 10 Ωcm samples were further used to conduct contact resistivity measurements using the circular transfer length method as described in ref. [14]. The advantage of the circular TLM structures is the circumvention of leakage currents which do occur on the linear structures. It should be noted, however, that corrections should be made in order to account for measurement errors and artefacts, among which is the current flow through the bulk

silicon as described thoroughly in ref [15]. In order to account for these errors the data should be fitted using simulated data generated with the Quokka software developed by Fell et al [16]. An in-depth description of this correction method will be described elsewhere [17].

2.3. EDNA analysis

As described in the previous section the EDNA software developed by McIntosh et al. [13] was used to simulate the effective surface recombination velocity of the samples. In order to successfully analyse the samples, the part of the dopant profile that was diffused into the c-Si wafer was extracted from the data and used as input for the EDNA analysis. In order to keep the analysis as simple as possible, no Shockley-Read Hall recombination was assumed in the doped region and the SRH surface recombination was described using an effective surface recombination velocity S_{eff}, which described both the recombination at the Si/SiO$_x$ interface and in the poly-Si layer itself [18]. The S_{eff} value corresponding to the saturation current density from the QSSPC measurement was obtained by iteration.

3. Results and discussion

3.1. QSSPC analysis

The obtained data from the QSSPC measurements after anneal and hydrogen passivation can be found in Fig. 1. The J_0 values increase significantly with increasing annealing temperature, except for the thermal oxides, which have low J_0 values for all annealing temperatures. The lowest J_0 value found was 15 fA/cm^2 for the thermal oxide, with a corresponding iV$_{OC}$ value of 707 mV and an implied fill factor of 84%.
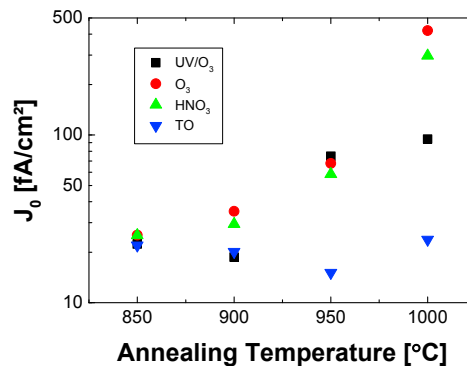

Fig. 1. Saturation current density values for each of the four oxides used during this study. The plotted data is obtained for the 10 Ωcm samples with a wafer thickness of 250 µm after hydrogen passivation.

From Fig. 1 is becomes clear that for the 850 °C anneal, all oxides show good passivation which results in a low saturation current density. If the annealing temperature increases, the J_0 increases rapidly for the O$_3$ and the HNO$_3$ oxides, indicating that the passivation deteriorates. The UV/O$_3$ oxide shows good passivation up to the 900 °C anneal, and thereafter also has deteriorated passivation. This behavior corresponds with earlier results found in literature [19]. The deterioration of the saturation current densities is likely explained by increased diffusion of the dopant atoms into the bulk material, possibly combined with a disintegration of the tunnel oxides. The passivation of the thermally grown oxide remains good even for the 1000 °C anneal, thus showing a higher thermal stability. Especially the 950 °C anneal shows an excellent passivation for the thermally grown oxide, with a saturation current density of 15 fA/cm^2.

3.2. ECV profiles & EDNA analysis

During the high temperature anneal, boron diffuses into the bulk material. The boron profiles were obtained by ECV measurements for all samples. The resulting dopant profiles for the samples annealed at 950 °C can be found in Fig. 2a.
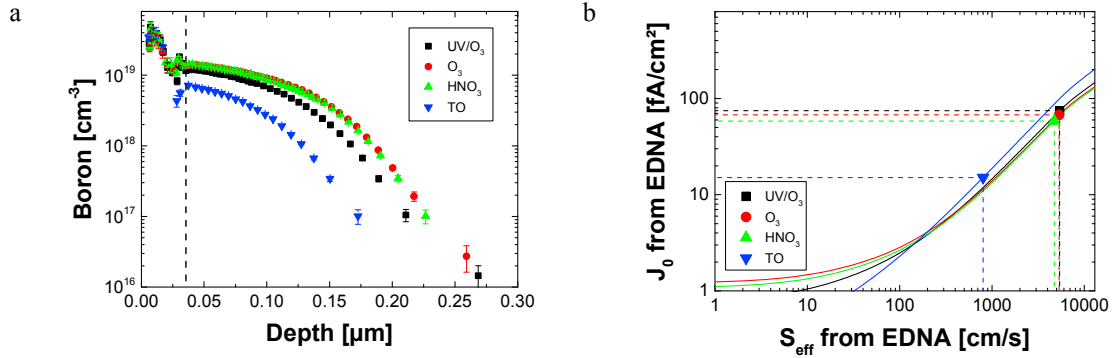

Fig. 2. (a) Measured ECV profiles for the samples annealed at 950 °C (b) EDNA analyses for the displayed ECV profiles.

From Fig. 2a, it becomes clear that the sample with a thermally grown oxide has both a shallower profile as well as a lower surface dopant concentration than the other three oxides. This means that less boron diffused through the thermal oxide compared to the other oxides. The O_3 and HNO_3 oxides show a very similar dopant profile, and also show similar passivation as can be seen in Fig. 1. The UV/O_3 oxide shows a similar surface dopant concentration, but a slightly shallower profile. The profiles obtained during the ECV measurements were used to simulate the recombination behavior using the EDNA software from McIntosh et al. [13]. From the boron profiles, only the part in the c-Si material was used, which approximately starts at the dotted line in Fig. 2a. This profile was used to estimate the effective surface recombination velocities at the SiO_x/c-Si interface for the samples based on the J_0 values obtained through improved Kane & Swanson analysis on the QSSPC data [12].

Fig. 2b shows the resulting J_0 versus S_{eff} curves for the samples annealed at 950 °C. The lowest effective surface recombination velocity occurs for the thermal oxide as indicated by the dotted lines. These lower values might be due to the lower surface concentration of dopants for this oxide or because other properties (like interface defects, trapped charge density at the interface and hydrogenation) are superior to the other three oxides. Furthermore, if very low S_{eff} values would be achieved, the J_0 would drop below 1 fA/cm^2, indicating that all profiles show negligible Auger recombination and that the saturation current density is limited by the SRH recombination at the interface. Finally, all curves show a strong dependence of J_0 on S_{eff}, indicating that all profiles are "transparent" and do not shield highly recombination active surfaces.

The saturation current density is plotted against the Seff values obtained from EDNA in Fig. 3 for all processed samples. From Fig. 3 a clear trend is observed: for each annealing temperature the samples with thermal oxide consistently show the lowest values for the effective surface recombination. Furthermore, it is evident that an increasing annealing temperature leads to an increasing J_0 and S_{eff} for all oxides, except for the thermal oxide. Thus, the quality of the tunnel oxide is essential for good passivation and the thermally grown oxide enables low surface recombination velocity values even at higher annealing temperatures.
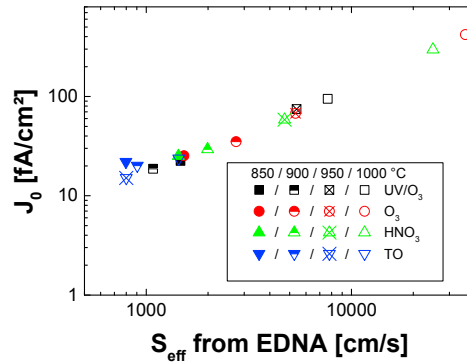
Fig. 3. Plot of J_0 versus S_{eff} for the four oxides at all annealing temperatures.

3.3. TLM measurements

The circular transfer length method (TLM) was used to determine the contact resistivity of the samples. The resulting values for the contact resistivity can be found in Fig. 4.
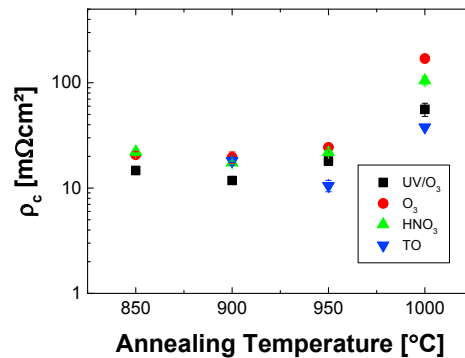

Fig. 4. Contact resistivity values for the TLM samples metallized with the TiPdAg layer.

From Fig. 4 we see that all oxides provide a reasonable specific contact resistivity value for the low annealing temperatures. However, for the higher annealing temperatures, the thermally grown oxide yields the lowest contact resistivity values. The best value is obtained at the 950 °C anneal, where the thermally grown oxide shows a specific contact resistivity value of 10 mΩcm^2, also the sample with the best passivation.

All oxides show an increased contact resistivity at an annealing temperature of 1000 °C, which is an unexpected effect. It would be expected to see a decrease in contact resistivity with increased annealing temperature due to oxide break-up and enhanced dopant diffusion into the bulk as it was reported for *n*-type TOPCon with HNO$_3$ oxide in ref. [20]. A possible explanation of this could be that a parasitic oxide grew onto the SiC capping layer during the annealing process. The unwanted oxidation of SiC can result in the growth of SiO$_x$C$_y$ which is fairly stable in HF [21]. During the TLM masking process a 30 second dip in a 1% hydrofluoric acid solution was used to remove the parasitic oxide, but this might not be sufficient for the 1000 °C anneal, leading to an increased contact resistivity between the TiPdAg metal stack and the doped silicon layer.

4. Conclusions

The thermally grown oxides prove to be a promising candidate for improved passivation of p-type carrier-selective contacts. They provide a low saturation current density of 15 fA/cm^2, combined with a low contact resistivity value of 10 mΩcm^2. This makes the performance of the thermally grown oxide better than the UV/O$_3$ oxide. Furthermore, this good passivation is maintained at higher annealing temperatures up to a 1000 °C. All oxides provide a reasonable contact resistivity. Remarkably, the contact resistivity increases for these very high annealing temperatures. This could be caused by parasitic oxide growth during the high temperature anneal which increases the contact resistivity between the metal and the TOPCon layer.

Acknowledgments

References

[1] Yoshikawa K, Kawasaki H, Yoshida W, Irie T, Konishi K, Nakano K, Uto T, Adachi D, Kanematsu M, Uzu H, Yamamoto K. Silicon heterojunction solar cell with interdigitated back contacts for a photoconversion efficiency over 26%. Nature Energy 2017;2:17032,

[2] Peibst R, Romer U, Larionova Y, Schulte-Huxel H, Ohrdes T, Haberle M, Lim B, Krugener J, Stichtenoth D, Wutherich T, Schollhorn C, Graff J, Brendel R. Building blocks for back-junction back-contacted cells and modules with ion-implanted poly-Si junctions. In: 40th IEEE Photovoltaic Specialists Conference (PVSC); 2014, p. 852–6.

[3] Römer U, Peibst R, Ohrdes T, Lim B, Krügener J, Bugiel E, Wietler T, Brendel R. Recombination behavior and contact resistance of n+ and p+ poly-crystalline Si/mono-crystalline Si junctions. Sol. Energy Mater. Sol. Cells 2014;131:85–91

[4] Feldmann F, Bivour M, Reichel C, Hermle M, Glunz SW. Passivated rear contacts for high-efficiency n-type Si solar cells providing high interface passivation quality and excellent transport characteristics. Sol. Energy Mater. Sol. Cells 2014;120:270–4

[5] Richter A, Benick J, Feldmann F, Fell A, Hermle M, Glunz SW. (in press). n-Type Si solar cells with passivating electron contact: Identifying sources for efficiency limitations by wafer thickness and resistivity variation. Sol. Energy Mater. Sol. Cells

[6] Kobayashi H, Imamura K, Kim W-B, Im S-S, Asuha. Nitric acid oxidation of Si (NAOS) method for low temperature fabrication of SiO2/Si and SiO2/SiC structures. Appl Surf Sci 2010;256:5744–56

[7] Moldovan A, Feldmann F, Krugel G, Zimmer M, Rentsch J, Hermle M, Roth-Fölsch A, Kaufmann K, Hagendorf C. Simple cleaning and conditioning of silicon surfaces with UV/Ozone sources. Energy Procedia 2014;55:834–44

[8] Fink CK, Nakamura K, Ichimura S, Jenkins SJ. Silicon oxidation by ozone. Journal of Physics: Condensed Matter 2009;21:183001

[9] Lindekugel S, Lautenschlager H, Ruof T, Reber S. Plasma hydrogen passivation for crystalline silicon thin-films. In: 23rd EU PVSEC; 2008, p. 2232–5.

[10] Sinton RA, Cuevas A, Stuckings M. Quasi-steady-state photoconductance, a new method for solar cell material and device characterization. In: 25th IEEE Photovoltaic Specialists Conference Washington DC; 1996, p. 457–60.

[11] Kane DE, Swanson RM. Measurement of the emitter saturation current by a contactless photoconductivity decay method (silicon solar cells). In: 18th IEEE Photovoltaic Specialists Conference Las Vegas; 1985, p. 578–83.

[12] Kimmerle A, Rothhardt P, Wolf A, Sinton RA. Increased reliability for J0-analysis by QSSPC. Energy Procedia 2014;55:101–6

[13] McIntosh KR, Altermatt PP. A freeware 1d emitter model for silicon solar cells. In: 35th IEEE Photovoltaic Specialists Conference Honolulu; 2010, p. 1–6.

[14] Schroder DK. Semiconductor material and device characterization. 3rd ed. Hoboken, New Jersey, USA: John Wiley & Sons; 2006.

[15] Eidelloth S, Brendel R. Analytical theory for extracting specific contact resistances of thick samples from the transmission line method. IEEE Electron Device Lett. 2014;35:9–11

[16] Fell A. A free and fast three-dimensional/two-dimensional solar cell simulator featuring conductive boundary and quasi-neutrality approximations. IEEE Trans. Electron Devices 2013;60:733–8

[17] Kökbudak G., Müller R., Feldmann F, Fell A., Turan R., Glunz SW. On the determination of the contact resistivity for passivating contacts using 3D simulations. In: 33rd European Photovoltaic Solar Energy Conference and Exhibition.

[18] Yan D, Cuevas A, Wan Y, Bullock J. Passivating contacts for silicon solar cells based on boron-diffused recrystallized amorphous silicon and thin dielectric interlayers. Sol. Energy Mater. Sol. Cells 2016;152:73

[19] Moldovan A, Feldmann F, Zimmer M, Rentsch J, Benick J, Hermle M. Tunnel oxide passivated carrier-selective contacts based on ultra thin SiO$_2$ layers: To be published. Sol. Energy Mater. Sol. Cells 2015.

[20] Feldmann F. Advanced Passivated Contacts and Their Applications to High-efficiency Cells. In: 25th Workshop on Crystalline Silicon Solar Cells & Modules: Materials and Processes.

[21] Schnabel M, Löper P, Gutsch S, Wilshaw PR, Janz S. Thermal oxidation and encapsulation of silicon–carbon nanolayers. Thin Solid Films 2013;527:193–9